DE GRUYTER
OPEN

Contributions to Geophysics and Geodesy Vol. 47/2, 2017 (113–132)

# Depth and shape solutions from residual gravity anomalies due to simple geometric structures using a statistical approach

El-Sayed ABDELRAHMAN, Mohamed GOBASHY

Geophysics Department, Faculty of Science, Cairo University, Egypt; e-mail: sayed5005@yahoo.com, bouguer3000@yahoo.com

**Abstract:** We have developed a simple and fast quantitative method for depth and shape determination from residual gravity anomalies due to simple geometrical bodies (semi-infinite vertical cylinder, horizontal cylinder, and sphere). The method is based on defining the anomaly value at two characteristic points and their corresponding distances on the anomaly profile. Using all possible combinations of the two characteristic points and their corresponding distances, a statistical procedure is developed for automated determination of the best shape and depth parameters of the buried structure from gravity data. A least-squares procedure is also formulated to estimate the amplitude coefficient which is related to the radius and density contrast of the buried structure. The method is applied to synthetic data with and without random errors and tested on two field examples from the USA and Germany. In all cases examined, the estimated depths and shapes are found to be in good agreement with actual values. The present method has the capability of minimizing the effect of random noise in data points to enhance the interpretation of results.

**Key words:** gravity interpretation, simple structures, standard deviation, noise

## 1. Introduction

The aim of gravity survey is to determine the depth and shape of buried structures of economic interest which reveal themselves as anomalies on the maps or the profiles. The measured anomalies are often used in a qualitative way to assist regional geological interpretations. However, sometimes an individual residual anomaly is found which stands out so clearly that it can be separated from the regional background and the neighbouring interferences (*Nettleton, 1976*) and which is so simple in appearance that it can be considered as caused by a single structure. In this case, quantitative

doi: 10.1515/congeo-2017-0008 

methods of interpretation can be used to determine the depth and shape of the buried structure.

The 2D (*Tanner, 1967*), 2.5 (*Chakravarthi, 2011*) or 3D (*Cordell and Henderson, 1968; Götze and Lahmeyer, 1988*) continuous modelling techniques are widely used to interpret gravity data. However, they are involved with personal prejudices and judgements as well as requiring density information as part of the input, along with some depth information obtained from geological and/or other geophysical data. Thus, the resulting model can vary widely, depending on these factors, and still give a calculated curve in close agreement with the observed data. On the other hand, the advantage of fixed geometry (spheres and cylinders) methods over continuous modelling methods is that they require neither density nor depth information and they can be applied if little or no factual information other than the gravity data is available. The models may not be geologically realistic, but usually approximate equivalence is sufficient to determine whether the form and magnitude of calculated gravity effects are close enough to the observed gravity data to make the geological postulate reasonable. Moreover, for interpreting simple geological structures, fixed geometry methods can be both fast and accurate.

Simultaneous estimation of the depth and shape of a buried structure from a residual gravity anomaly profile due to simple geological structure has drawn considerable attention. The methods generally fall into one of two categories. The first category is the convolution methods, in which simple models are convolved with the same moving average filters or numerical horizontal derivative filters as applied to the observed gravity data (e.g. *Abdelrahman and El-Araby, 1996; Abdelrahman et al., 2001a & 2006*), and correlation factors between successive least-squares residual gravity anomalies (*Abdelrahman and El-Araby, 1993*). These methods can be applied to both residual and observed data. However, the convolution and correlation methods may be excluded when interpreting a residual gravity anomaly due to a purely local structure because these methods are highly sensitive to errors in the anomaly amplitude resolution and they are lengthy and tedious.

The second category is the methods which can be applied only to residual gravity anomaly due to a purely local structure to estimate the shape and depth. The methods include, for example, the Walsh transform technique (*Shaw and Agarwal, 1990*), use of quadratic equations (*Nandi et al., 1997*),

least-squares minimization approaches (*Abdelrahman and Sharafeldin, 1995; Abdelrahman et al., 2001b; Essa, 2014*), iterative methods (*Abdelrahman and El-Araby, 1996*), constrained and penalized nonlinear optimization techniques (*Tlas et al., 2005*), use of a common intersection point of depth curves (*Essa, 2007*), non-convex and nonlinear Fair function minimization, adaptive simulated annealing, and stochastic optimization algorithm (*Asfahani and Tlas, 2012*), deconvolution technique and use of simplex algorithm for linear optimization (*Asfahani and Tlas, 2015*). However, most of these methods, particularly those given by *Abdelrahman and Sharafeldin (1995)*, *Abdelrahman et al. (2001b)*, *Abdelrahman and El-Araby (1996)* and *Essa (2007 & 2014)* are based on defining the anomaly value at the origin [g(max)] and it remains as a fixed parameter in the process, and hence they are highly subjective in determining the shape and depth of the buried structure from the residual gravity anomaly profile.

To address the above problem and to make the problem computationally tractable on a personal computer, a simple and fast statistical method to determine the depth and shape of a buried structure from a residual gravity anomaly profile, has been developed. The method uses all possible combinations of two characteristic points and their corresponding distances for automated determination of the best shape and depth parameters of the buried structure from gravity data. The advantage of the present technique over nonlinear least-squares methods and depth-shape curves methods (*Abdelrahman et al., 2001b & 2006; Abdelrahman and El-Araby, 1996; Essa, 2007 & 2014*), is that it has the capability of minimizing the effect of random errors in the data points to enhance the interpretation results because the method uses all successful combinations of data points several times. When our statistical approach is used, the use of anomaly value at the origin plays a minor role in determining the model parameters. The method is applied to synthetic data with and without random errors and tested on two field examples from the USA and Germany.

## 2. Theory

The general gravity anomaly expressions produced by a sphere, an infinitely long horizontal cylinder, and a semi-infinite vertical cylinder can be given as (*Abdelrahman et al., 2001a*):

$$g(x,z,q) = \frac{A}{(x^2 + z^2)^q}\,, \tag{1}$$

where

$$A = \begin{cases} \pi\, G\rho\, R^2 & [\text{mGal} \cdot \text{depth unit}] \\ 2\pi\, G\rho\, R^2 z & [\text{mGal} \cdot (\text{depth unit})^2] \\ (4/3)\pi\, G\rho R^3 z & [\text{mGal} \cdot (\text{depth unit})^3]\,, \end{cases}$$

$$q = \begin{cases} 0.5 & \text{for a semi-infinite vertical cylinder} \\ 1.0 & \text{for a horizontal cylinder} \\ 1.5 & \text{for a sphere}\,. \end{cases}$$

In equation (1), $z$ is the depth of the body, $x$ is the position coordinate, $A$ is the amplitude coefficient related to the density contrast ($\rho$) and the radius ($R$) of the buried structure, $q$ is the shape value and $G$ is the universal gravitational constant.

For all shapes ($q$), equation (1) gives the following two equations at $x_i$ and $x_j$ respectively:

$$g(x_i) = \frac{A}{(x_i^2 + z^2)^q}, \tag{2}$$

$$g(x_j) = \frac{A}{(x_j^2 + z^2)^q}, \tag{3}$$

where $x_i$ and $x_j$ are two different horizontal distances from the point of the origin to the point where the residual gravity has $g(x_i)$ and $g(x_j)$ values, respectively.

Let $L = g(x_i)/g(x_j)$, then using equations (2), and (3), we obtain:

$$z = \sqrt{\frac{L^{1/q} x_i^2 - x_j^2}{1 - L^{1/q}}}\,. \tag{4}$$

For all shapes, equation (4) will converge to a depth solution when $x_i \neq x_j$, $x_i + x_j \neq 0$, $L^{1/q} < 1$, and $x_j^2 < x_i^2 L^{1/q}$. These conditions should be implemented in any computer program in order to determine a reliable depth estimate from all successful combinations of $x_i$ and $x_j$. Theoretically, one successful value of $x_i$ and $x_j$ is sufficient to determine the depth to the buried structure from equation (4), but in practice, more successful

combinations of $x_i$ and $x_j$ are desirable because of the presence of noise in the data. However, equation (4) can also be used not only to determine the depth but also to estimate simultaneously the shape of the buried structure. The procedure is as follows:

1) Digitize the residual anomaly profile at several points including the central point $x = 0$.
2) For each $x_i$ and $x_j$ value, apply equation (4) to the residual anomaly profile, yielding depth solutions ($z$) for all possible $q$ values. We then compute the standard deviation of depths for each value of ($q$).
3) Finally, we use a search algorithm to find the value of ($q$) at which the standard deviation of the depths is a minimum.

The minimum standard deviation is used as a criterion for determining the correct depth and the shape of the buried structure. When the correct value of the shape is used, the standard deviation of the depths is always less than the standard deviations computed using wrong values of ($q$).

Knowing the computed depth ($z_c$) and shape value ($q_c$), and applying the least-squares method to equation (1), the amplitude coefficient ($A$) can be determined from:

$$A = \frac{\sum_{k=1}^{N} \frac{D(x_k)}{(x_k^2 + z_c^2)^{q_c}}}{\sum_{k=1}^{N} \frac{1}{(x_k^2 + z_c^2)^{2q_c}}}, \tag{5}$$

where $D(x_k)$ is the observed residual gravity anomaly.

## 3. Theoretical examples

### 3.1. Noise Free Data

We have computed three different residual gravity anomalies due to a semi-infinite vertical cylinder ($A_1 = 20$ mGal·km, $z = 4$ km, and $q = 0.5$), a horizontal cylinder ($A_2 = 500$ mGal·km$^2$, $z = 6$ km, and $q = 1$), and a sphere ($A_3 = 15000$ mGal·km$^3$, $z = 10$ km, $q = 1.5$). Figure 1 shows the residual gravity anomalies computed from the following model equations:

$$g(x) = \frac{A_1}{(x^2 + 4^2)^{0.5}} \quad \text{for the semi-infinite vertical cylinder,} \tag{6}$$

$$g(x) = \frac{A_2}{(x^2 + 6^2)} \quad \text{for the horizontal cylinder,} \tag{7}$$

$$g(x) = \frac{A_3}{(x^2 + 10^2)^{1.5}} \quad \text{for the sphere.} \tag{8}$$

Equation (4) has been applied to each residual anomaly profile, yielding depth solutions for all possible $q$ values (0.1, 0.2, 0.3, ..., and 2.0) for all successful combinations of $x_i$ and $x_j$ (200 combinations). We then computed the standard deviation of the depths for each shape value. The depths, their average values, and their standard deviations are given in Table 1.

Table 1. Numerical results otained from the gravity anomaly due to a semi-infinite vertical cylinder ($z$ = 4 km and $q$ = 0.5), a horizontal cylinder ($z$ = 6 km and $q$ = 1.0),and a sphere ($z$ = 10 km and $q$ = 1.5). Number of successful combinations = 200 (best results in bold).

| Model | Semi-infinite vertical cylinder | | Horizontal cylinder | | Sphere | |
|---|---|---|---|---|---|---|
| Shape value (q) | Average depth value (km) | Standard deviation | Average depth value (km) | Standard deviation | Average depth value (km) | Standard deviation |
| 0.1 | 22.291 | 8.7378 | 22.287 | 8.7496 | 20.866 | 9.9121 |
| 0.2 | 17.974 | 11.452 | 19.94 | 10.471 | 17.235 | 11.471 |
| 0.3 | 11.995 | 11.795 | 16.212 | 11.791 | 13.333 | 11.565 |
| 0.4 | 4.5771 | 6.3103 | 13.17 | 11.707 | 10.095 | 10.352 |
| **0.5** | **4.0000** | **0.0000** | 9.2521 | 10.381 | 7.9602 | 8.4432 |
| 0.6 | 5.0021 | 0.40715 | 6.5126 | 7.851 | 6.378 | 5.8463 |
| 0.7 | 5.8356 | 0.69118 | 4.4025 | 3.175 | 5.7869 | 3.0532 |
| 0.8 | 6.568 | 0.91797 | 4.7338 | 0.46357 | 6.1115 | 0.85552 |
| 0.9 | 7.2296 | 1.1107 | 5.4075 | 0.19556 | 6.8126 | 0.638 |
| **1** | 7.8377 | 1.2805 | **6.0000** | **0.00000** | 7.4417 | 0.47992 |
| 1.1 | 8.4036 | 1.4335 | 6.538 | 0.15791 | 8.0196 | 0.35353 |
| 1.2 | 8.9349 | 1.5739 | 7.035 | 0.29214 | 8.5579 | 0.24733 |
| 1.3 | 9.4372 | 1.704 | 7.4996 | 0.40994 | 9.0641 | 0.15523 |
| 1.4 | 9.9148 | 1.8258 | 7.9376 | 0.51557 | 9.5435 | 0.073581 |
| **1.5** | 10.371 | 1.9407 | 8.353 | 0.61181 | **10.0000** | **0.00000** |
| 1.6 | 10.808 | 2.0497 | 8.7492 | 0.70053 | 10.437 | 0.067149 |
| 1.7 | 11.229 | 2.1535 | 9.1286 | 0.7831 | 10.856 | 0.12905 |
| 1.8 | 11.635 | 2.2529 | 9.4931 | 0.86053 | 11.26 | 0.18657 |
| 1.9 | 12.027 | 2.3483 | 9.8443 | 0.93357 | 11.649 | 0.24039 |
| 2.0 | 12.407 | 2.4401 | 10.184 | 1.0028 | 12.027 | 0.29103 |

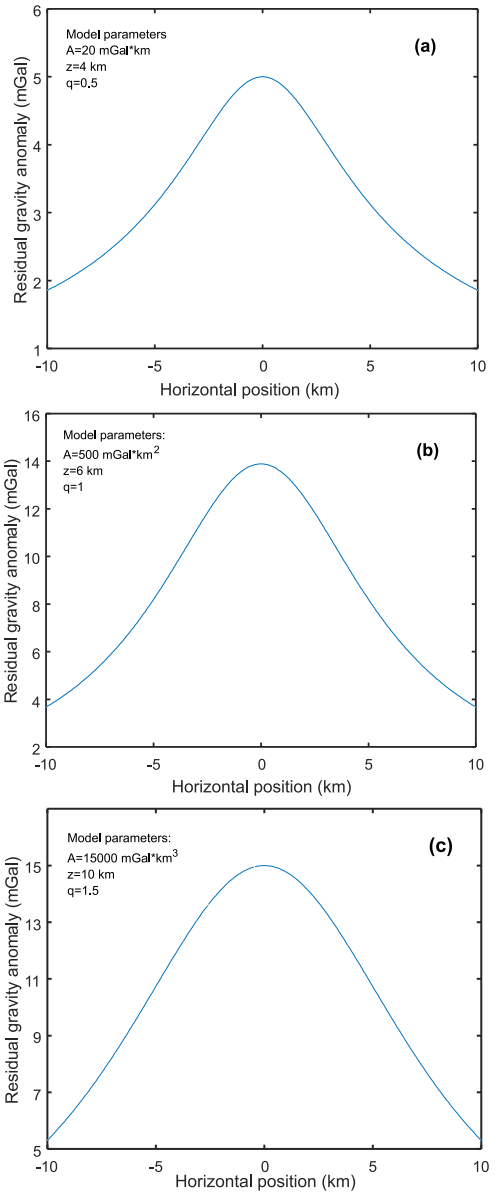


Fig. 1. A gravity anomaly over (a) a semi-infinite vertical cylinder ($A_1 = 20$ mGal·km, $z = 4$ km, and $q = 0.5$); (b) a horizontal cylinder ($A_2 = 500$ mGal·km$^2$, $z = 6$ km, and $q = 1$); and (c) a sphere ($A_3 = 15000$ mGal·km$^3$, $z = 10$ km, and $q = 1.5$).

The result of this study shows that the correct solution for the semi-infinite vertical cylinder model ($z = 4$ m, and $q = 0.5$), the horizontal cylinder model ($z = 6$ km and $q = 1$), and the sphere model ($z = 10$ km and $q = 1.5$) occurs at zero standard deviation of the depths. The zero value of the standard deviation is expected because the computed depths from the residual anomaly profile using all successful combinations of $x_i$ and $x_j$ are equal to the true depth of the model when the correct shape value is used. The computed depth and the shape are in excellent agreement with the actual depth and shape of each model.

### 3.2. Effect of Random Noise

To test the stability of our method in the presence of noise, 10% random errors were added to each residual gravity anomaly to produce noisy data (Figure 2). Following the same interpretation method, the results of all successful combinations (90) are shown in Table 2.

Table 2 shows that when the data contain 10% random errors, the minimum standard deviation occurs at $z = 4.36$ km and $q = 0.5$ for the semi-infinite vertical cylinder model, $z = 6.42$ km and $q = 1.1$, for the horizontal cylinder model, and $z = 9.98$ km and $q = 1.4$ for the sphere model. This demonstrates that the present method will give reliable model parameters ($z$ and $q$) even when the residual gravity anomaly is contaminated with random errors.

### 3.3. Effect of Wrong Origin

This procedure begins with selecting the origin ($x = 0$) where the residual anomaly attains its maximum value and may lead to errors in the depth and shape when interpreting real data. This occurs when precise residual anomalies are not available, and when the anomalies are not well isolated from each other and when the sources are not truly idealized. We investigate this problem in this subsection.

We have computed a residual gravity anomaly due to a semi-infinite vertical cylinder ($q = 0.5$) buried at depths of 4 km and 6 km. We have introduced error of $\pm 50$, $\pm 100$ m, and $\pm 150$ m to the horizontal coordinate.

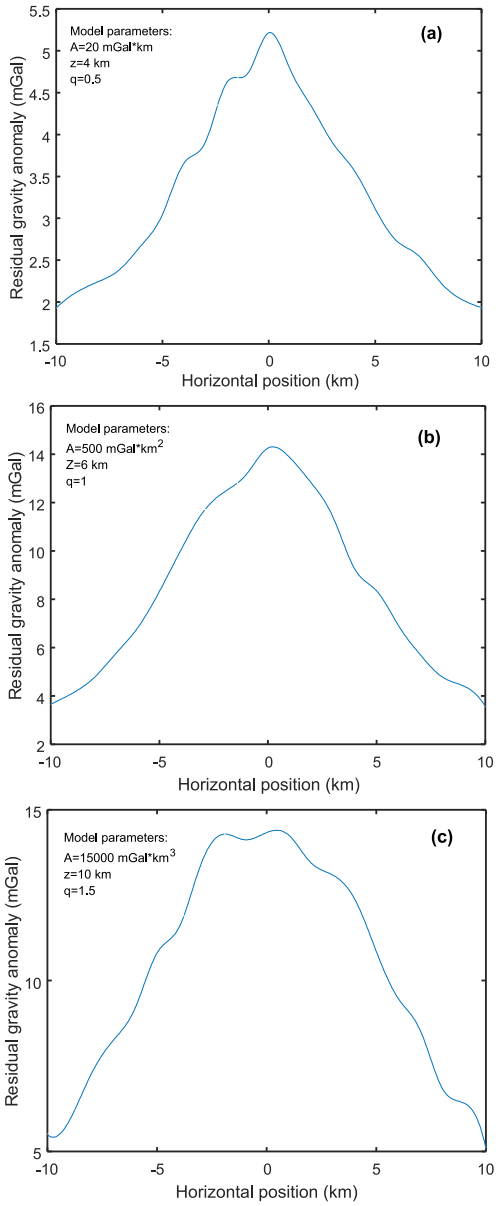


Fig. 2. A noisy gravity anomaly over (a) a semi-infinite vertical cylinder ($A_1 = 20$ mGal·km, $z = 4$ km, and $q = 0.5$); (b) a horizontal cylinder ($A_2 = 500$ mGal·km$^2$, $z = 6$ km, and $q = 1$); and (c) a sphere ($A_3 = 15000$ mGal·km$^3$, $z = 10$ km, and $q = 1.5$).

Table 2. Numerical results otained from the noisy gravity anomaly due to a semi-infinite vertical cylinder ($z = 4$ km and $q = 0.5$), a horizontal cylinder ($z = 6$ km and $q = 1.04$), and a sphere ($z = 10$ km and $q = 1.5$). Number of successful combinations = 90 (best results in bold).

| Model | Semi-infinite vertical cylinder | | Horizontal cylinder | | Sphere | |
|---|---|---|---|---|---|---|
| Shape value (q) | Average depth value (km) | Standard deviation | Average depth value (km) | Standard deviation | Average depth value (km) | Standard deviation |
| 0.1 | 22.425 | 8.6721 | 22.439 | 8.638 | 20.678 | 9.9799 |
| 0.2 | 17.355 | 11.73 | 20.631 | 10.067 | 16.965 | 11.438 |
| 0.3 | 9.7093 | 11.179 | 16.729 | 11.725 | 13.188 | 11.396 |
| 0.4 | 3.9499 | 4.1582 | 13.01 | 11.787 | 9.888 | 10.006 |
| **0.5** | **4.356** | **0.99297** | 10.265 | 10.802 | 7.745 | 7.9343 |
| 0.6 | 5.3436 | 1.1693 | 6.5951 | 7.9913 | 6.7453 | 5.7781 |
| 0.7 | 6.1779 | 1.3738 | 4.1538 | 2.5166 | 6.7707 | 4.4086 |
| 0.8 | 6.9171 | 1.565 | 4.9336 | 2.3652 | 6.9869 | 3.2699 |
| 0.9 | 7.5883 | 1.7409 | 5.5815 | 2.2877 | 7.4291 | 2.5024 |
| 1 | 8.2073 | 1.9036 | 6.1563 | 2.239 | 8.0701 | 2.4071 |
| **1.1** | 8.7846 | 2.0551 | **6.4226** | **0.93677** | 8.3812 | 1.6631 |
| 1.2 | 9.3276 | 2.1973 | 6.9227 | 0.96346 | 8.9525 | 1.581 |
| 1.3 | 9.8416 | 2.3316 | 7.3878 | 1.0144 | 9.4809 | 1.5565 |
| **1.4** | 10.331 | 2.4591 | 7.8255 | 1.0743 | **9.9796** | **1.5498** |
| 1.5 | 10.799 | 2.5806 | 8.2403 | 1.1378 | 10.454 | 1.5532 |
| 1.6 | 11.247 | 2.697 | 8.6355 | 1.2023 | 10.907 | 1.5632 |
| 1.7 | 11.679 | 2.8088 | 9.0138 | 1.2664 | 11.342 | 1.5778 |
| 1.8 | 12.096 | 2.9164 | 9.3772 | 1.3296 | 11.761 | 1.5955 |
| 1.9 | 12.499 | 3.0204 | 9.7274 | 1.3915 | 12.165 | 1.6156 |
| 2.0 | 12.89 | 3.121 | 10.066 | 1.4519 | 12.557 | 1.6375 |

We applied our interpretation method to the residual anomalies thus obtained. The results are shown in Table 3 and 4.

In the case that the actual depth to the buried vertical cylinder is 4 km, the minimum standard deviation occurs at $z = 4$ km and $q = 0.5$; $z = 5.02$ km, and $q = 0.6$; and $z = 5.03$ km, and $q = 0.6$, when the offset is $\pm 50$ m, $\pm 100$ m, and $\pm 150$ m, respectively (Table 3). The error in depth and shape value is about 10%. However, in case that the actual depth is 6 km, the minimum standard deviation occurs at $z = 6.004$ m and $q = 0.5$; $z = 6.016$ km, and $q = 0.5$; and $z = 6.04$ km, and $q = 0.5$, when the offset is $\pm 50$, $\pm 100$ m, and $\pm 150$ m respectively (Table 4). In this case, the computed

Table 3. Numerical results otained from the gravity anomaly due to a semi-infinite vertical cylinder ($z = 4$ km and $q = 0.5$, after introducing error of ±50 m, ±100 m, and ±150 m to the horizontal coordinate. Number of successful combinations= 995, (best result in bold).

| Offset | 50 m | | 100 m | | 150 m | |
|---|---|---|---|---|---|---|
| Shape value (q) | Average depth value (km) | Standard deviation (km) | Average depth value (km) | Standard deviation (km) | Average depth value (km) | Standard deviation (km) |
| 0.1 | 22.2913 | 8.737471 | 22.29174 | 8.736526 | 22.1653 | 8.8677 |
| 0.2 | 17.97676 | 11.4485 | 18.11182 | 11.38144 | 17.99254 | 11.42597 |
| 0.3 | 12.25692 | 11.80837 | 12.02437 | 11.7686 | 11.6936 | 11.68509 |
| 0.4 | 4.478177 | 6.124505 | 5.03334 | 6.776616 | 5.204922 | 6.925853 |
| **0.5** | **4.000003** | **0.265515** | 4.123866 | 1.622493 | 4.391082 | 2.736029 |
| **0.6** | 5.005333 | 0.466841 | **5.015129** | **0.61759** | **5.031609** | **0.825259** |
| 0.7 | 5.839765 | 0.726825 | 5.852389 | 0.828216 | 5.874366 | 0.985367 |
| 0.8 | 6.572619 | 0.945842 | 6.586808 | 1.02802 | 6.611555 | 1.162123 |
| 0.9 | 7.234566 | 1.13494 | 7.249915 | 1.207622 | 7.276685 | 1.329435 |
| 1 | 7.843026 | 1.302718 | 7.859348 | 1.370045 | 7.88781 | 1.484705 |
| 1.1 | 8.409171 | 1.454607 | 8.426358 | 1.51869 | 8.456326 | 1.628987 |
| 1.2 | 8.940717 | 1.594164 | 8.958698 | 1.65621 | 8.990051 | 1.763808 |
| 1.3 | 9.443276 | 1.723833 | 9.462002 | 1.784591 | 9.494651 | 1.89055 |
| 1.4 | 9.921089 | 1.845365 | 9.94052 | 1.90533 | 9.974396 | 2.010361 |
| 1.5 | 10.37745 | 1.960064 | 10.39756 | 2.019574 | 10.4326 | 2.124173 |
| 1.6 | 10.81499 | 2.068924 | 10.83574 | 2.128223 | 10.87192 | 2.232745 |
| 1.7 | 11.23584 | 2.172725 | 11.25721 | 2.23199 | 11.29447 | 2.336698 |
| 1.8 | 11.64176 | 2.272092 | 11.66373 | 2.331455 | 11.70204 | 2.436547 |
| 1.9 | 12.03421 | 2.367531 | 12.05677 | 2.427095 | 12.0961 | 2.53272 |
| 2.0 | 12.41445 | 2.459462 | 12.43758 | 2.519304 | 12.4779 | 2.625581 |

shape value is in excellent agreement with the actual one and the error is less than 1% on the depth.

It is verified numerically that in most cases, the present method will give reasonable model parameters ($z$ and $q$) when the offset of the origin of the residual anomaly profile is small and particularly when the depth to the buried structure is relatively deep.

### 3.4. Extension to more complex shape

Consider, for example, the gravity field:

Table 4. Numerical results obtained from the gravity anomaly due to a semi-infinite vertical cylinder ($z = 6$ km and $q = 0.5$, after introducing error of ±50 m, ±100 m, and ±150 m to the horizontal coordinate. Number of successful combinations = 200, (best result in bold).

| Offset | 50 m | | 100 m | | 150 m | |
|---|---|---|---|---|---|---|
| Shape value (q) | Average depth value (km) | Standard deviation (km) | Average depth value (km) | Standard deviation (km) | Average depth value (km) | Standard deviation (km) |
| 0.1 | 19.93987 | 10.47232 | 20.06987 | 10.38274 | 19.94991 | 10.45508 |
| 0.2 | 12.91684 | 11.70444 | 12.80458 | 11.68851 | 12.70123 | 11.66414 |
| 0.3 | 6.394335 | 7.739274 | 6.573078 | 7.821957 | 6.373522 | 7.585099 |
| 0.4 | 4.732241 | 0.556722 | 4.860888 | 1.641535 | 5.008582 | 2.253349 |
| **0.5** | **6.003876** | **2.32E-01** | **6.015646** | **0.471295** | **6.035598** | **0.729651** |
| 0.6 | 7.039808 | 0.371306 | 7.054549 | 0.549541 | 7.080229 | 0.774445 |
| 0.7 | 7.942921 | 0.566489 | 7.959363 | 0.70237 | 7.988034 | 0.89833 |
| 0.8 | 8.755008 | 0.741341 | 8.772779 | 0.856725 | 8.803765 | 1.034602 |
| 0.9 | 9.499229 | 0.896441 | 9.518154 | 1.000791 | 9.551148 | 1.167733 |
| 1 | 10.19021 | 1.036012 | 10.21018 | 1.13E+00 | 10.245 | 1.294146 |
| 1.1 | 10.83794 | 1.163395 | 10.85889 | 1.25731 | 10.89541 | 1.413453 |
| 1.2 | 11.44961 | 1.281013 | 11.47148 | 1.37244 | 11.50961 | 1.526139 |
| 1.3 | 12.03063 | 1.390635 | 12.05338 | 1.480521 | 12.09303 | 1.632886 |
| 1.4 | 12.58517 | 1.493581 | 12.60875 | 1.582559 | 12.64986 | 1.734359 |
| 1.5 | 13.11652 | 1.590859 | 13.14091 | 1.679373 | 13.18343 | 1.831155 |
| 1.6 | 13.62737 | 1.683258 | 13.65253 | 1.771625 | 13.69641 | 1.923791 |
| 1.7 | 14.1199 | 1.771404 | 14.14582 | 1.85986 | 14.191 | 2.012707 |
| 1.8 | 14.59595 | 1.855805 | 14.62259 | 1.944526 | 14.66905 | 2.09828 |
| 1.9 | 15.05705 | 1.93688 | 15.08441 | 2.025999 | 15.13211 | 2.180833 |
| 2 | 15.50454 | 2.014973 | 15.53259 | 2.104597 | 15.58149 | 2.260644 |

$$g(x) = \frac{A_4}{(x^2 + 4^2)^{0.5}} - \frac{A_4}{(x^2 + 15^2)^{0.5}}\,, \tag{9}$$

which represents a gravity field caused by a finite vertical cylinder (vertical line approximation) with $A_4 = 200$ mGal·km, $z_1 = 4$ km, $z_2 = 15$ km and $q = 0.5$. Adapting the same procedure used in the above examples, the results are given in Table 5. The minimum standard deviation occurs at $z = 5.07$ km and $q = 1.0$. These results suggest that our interpretation method may extended to infer a distinction in shape between an infinite vertical cylinder ($q = 0.5$) and finite vertical cylinder ($q = \sim 1$) and sphere ($q = 1.5$).

Table 5. Numerical results obtained from the gravity anomaly due to a finite vertical cylinder ($z_1 = 4$ km, $z_2 = 15$ km, and $q = 0.5$). Number of successful combinations = 200 (best result in bold).

| Shape value (q) | Average depth value (km) | Standard deviation (km) |
|---|---|---|
| 0.1 | 22.76172 | 8.268753 |
| 0.2 | 20.83417 | 9.974456 |
| 0.3 | 18.50681 | 11.18468 |
| 0.4 | 15.29227 | 11.89993 |
| 0.5 | 12.21779 | 11.60309 |
| 0.6 | 8.766571 | 10.14627 |
| 0.7 | 5.970825 | 7.374289 |
| 0.8 | 4.254284 | 3.152769 |
| 0.9 | 4.478843 | 0.344384 |
| **1** | **5.076898** | **0.125388** |
| 1.1 | 5.606381 | 0.163368 |
| 1.2 | 6.089129 | 0.301223 |
| 1.3 | 6.536545 | 0.430123 |
| 1.4 | 6.955755 | 0.546314 |
| 1.5 | 7.351658 | 0.651905 |
| 1.6 | 7.727826 | 0.748911 |
| 1.7 | 8.086979 | 0.838886 |
| 1.8 | 8.431247 | 0.923008 |
| 1.9 | 8.762343 | 1.002182 |
| 2 | 9.081673 | 1.077111 |

## 4. Field Examples

To examine the applicability of the present method, the following two field examples are presented.

### 4.1. Humble dome anomaly

The Humble oil field is located near the town of Humble in north-eastern Harris County on the Upper Gulf Coast of Texas. Named for its location, the field has drawn oil from an anhydrite and limestone reservoir in the cap rock and on the flanks of a piercement salt dome in Eocene, Miocene, Oligocene, and Pliocene formations. Figure 3 (*Nettleton, 1962*) shows the Bouguer

gravity map of the Humble dome. Each dot on this map is representing a gravity station. Figure 4 is a profile on the line A–A' of the map. A regional trend is removed graphically to give the residual curve shown and

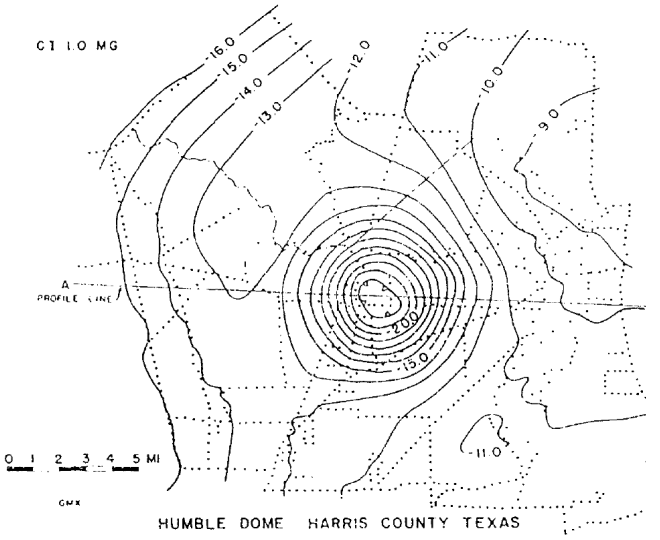


Fig. 3. Bouguer gravity map, Humble dome, near Houston, TX, USA (*Nettleton, 1962*).

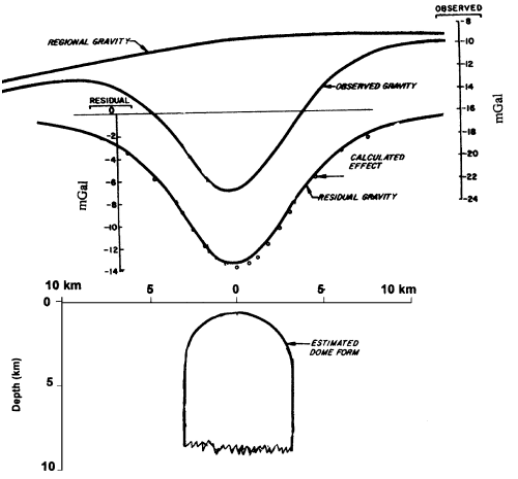


Fig. 4. Gravity profile on line AA' of the Humble dome, near Houston, TX, USA and the dome form as estimated from drilling and seismic data (*Nettleton, 1962*).

the application of our method is carried out on the central part of this residual anomaly profile (Figure 5). The anomaly profile (l6.62 km) was digitized at an interval of 0.277 km. Equation (4) was used to determine the depth and the shape of the buried salt dome using the present method. The result of using 995 successful combinations of $x_i$ and $x_j$ is given in Table 6. The minimum standard deviation occurs at $z = 5.05$ km and $q = 1.4$. The shape value thus obtained by the present method suggests that the shape of the 3-D source body can be represented by a finite vertical cylinder with a hemispherical roof. This is in good agreement with the dome form (Figure 4) estimated by *Nettleton (1962)*. Moreover, using equation (5) and knowing the depth and the shape value of the Humble dome, the amplitude coefficient A was found to be $-1254.6$ mGal·km$^{2.8}$. The observed and the calculated anomalies are shown in Figure 5.

Table 6. Numerical results of the Humble dome field example, USA. Number of successful combinations = 995 (best result in bold).

| Shape value (q) | Average depth value (km) | Standard deviation (km) |
|---|---|---|
| 0.1 | 20.55527 | 10.30866 |
| 0.2 | 18.64775 | 11.33881 |
| 0.3 | 16.16818 | 12.1071 |
| 0.4 | 13.51026 | 12.27788 |
| 0.5 | 11.07518 | 11.84324 |
| 0.6 | 8.801613 | 10.86976 |
| 0.7 | 6.907022 | 9.47108 |
| 0.8 | 5.447431 | 7.785582 |
| 0.9 | 4.795857 | 6.472268 |
| 1 | 4.590444 | 5.595233 |
| 1.1 | 4.489796 | 4.815234 |
| 1.2 | 4.642013 | 4.497059 |
| 1.3 | 4.819036 | 4.285611 |
| **1.4** | **5.047946** | **4.238352** |
| 1.5 | 5.334606 | 4.344278 |
| 1.6 | 5.604139 | 4.452039 |
| 1.7 | 5.860173 | 4.559678 |
| 1.8 | 6.104785 | 4.666555 |
| 1.9 | 6.339486 | 4.772349 |
| 2 | 6.565449 | 4.876888 |

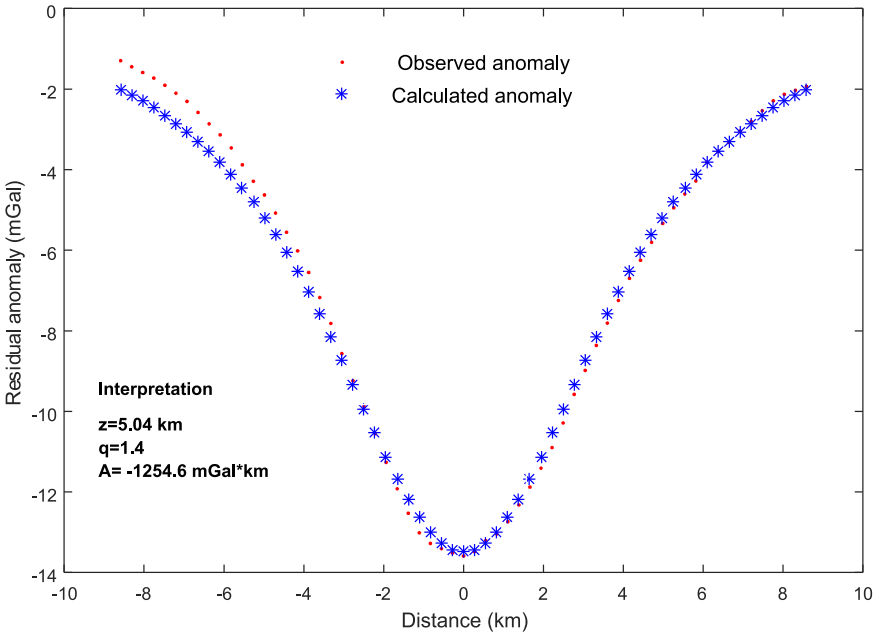


Fig. 5. A residual gravity anomaly over the Humble dome, near Houston, TX, USA.

### 4.2. Wathlingen dome anomaly

The Wathlingen salt dome is situated in the southern part of the Northwest German Basin. An excellent detailed review of the geology of the salt dome is given in *Dubey et al. (2014)*. It is evident that the peak of the salt diapirism in North Germany was probably at the end of the Late Jurassic and came to an end during the Lower Cretaceous. During the ascent of the salt, the overlying horizontal beds were heavily inclined. Figure 6 shows the observed gravity anomaly over the Wathlingen salt dome (*Dubey et al., 2014*). A central profile of a short length (5 km) of this anomaly was digitized at an interval of 50 m (Figure 7) and was used to determine the depth and the shape of the buried salt dome using the present method. The result of using 2500 successful combinations of $x_i$ and $\mathrm{x}_j$ is given in Table 7. The minimum standard deviation occurs at $z = 3.2$ km and $q = 1$. The shape value thus obtained by the present method suggests that the shape of the source body can be represented by a 2D horizontal cylinder buried

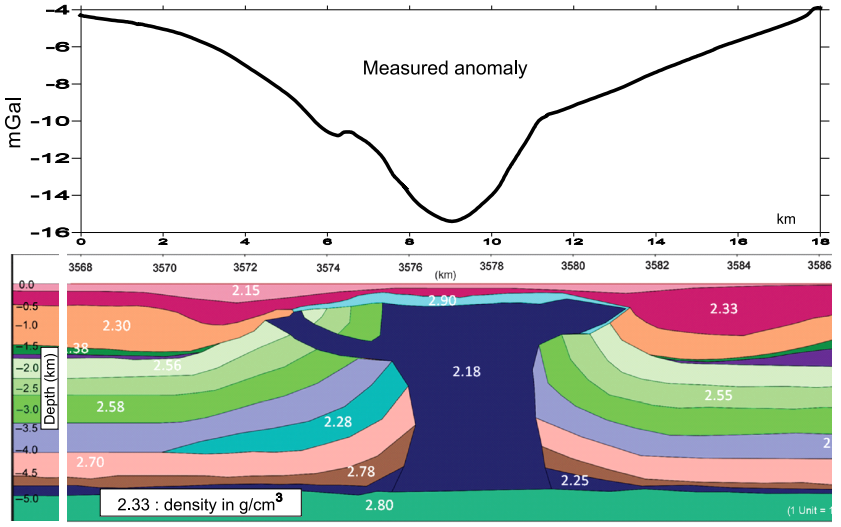


Fig. 6. Gravity profile over the Wathlingen dome, Germany, and the dome form as estimated from joint 3D modeling of gravity, gravity gradients, curvature derived from horizontal gradients and horizontal directive tendency, geological and borehole information (modified after *Dubey et al. (2014)*).

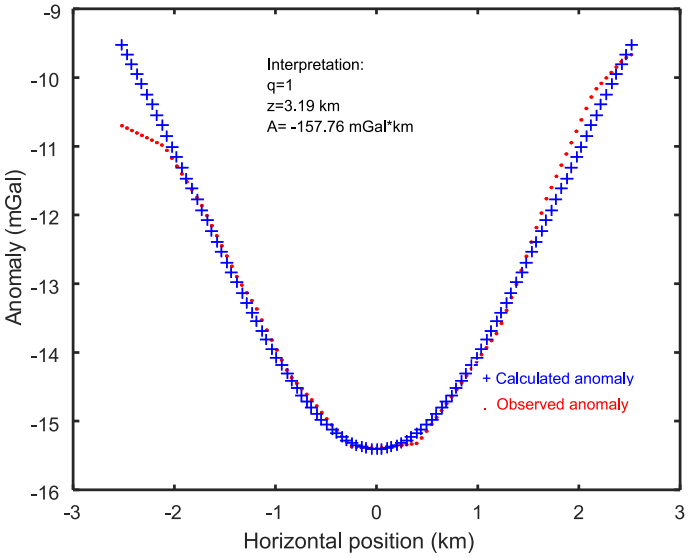


Fig. 7. A central gravity anomaly profile of 5 km length over the Wathlingen dome, Germany, as digitized from the gravity anomaly of Figure 6.

Table 7. Numerical results of the Wathlingene dome field example, Germany. Number of successful combinations =2500 (best result in bold).

| Shape value (q) | Average depth value (km) | Standard deviation (km) |
|---|---|---|
| 0.1 | 15.08667 | 12.43876 |
| 0.2 | 8.208308 | 11.256 |
| 0.3 | 2.689076 | 5.652535 |
| 0.4 | 2.167202 | 3.340847 |
| 0.5 | 2.24565 | 2.319903 |
| 0.6 | 2.430294 | 1.759949 |
| 0.7 | 2.613941 | 1.247812 |
| 0.8 | 2.815732 | 0.958196 |
| 0.9 | 3.0097 | 0.716992 |
| **1** | **3.199783** | **0.572868** |
| 1.1 | 3.38805 | 0.591558 |
| 1.2 | 3.566313 | 0.610804 |
| 1.3 | 3.736047 | 0.630149 |
| 1.4 | 3.898384 | 0.649383 |
| 1.5 | 4.054219 | 0.668395 |
| 1.6 | 4.20428 | 0.687129 |
| 1.7 | 4.349166 | 0.705553 |
| 1.8 | 4.489379 | 0.723655 |
| 1.9 | 4.625345 | 0.741433 |
| 2 | 4.757428 | 0.758888 |

at a depth of about 3.2 km. This is in good agreement with the dome form estimated by *Dubey et al. (2014)* who derived a 3D density model of the Wathlingen salt dome from joint modelling of gravity, gravity gradients, curvature derived from horizontal gradients and horizontal directive tendency, geological and borehole information. They found that the Wathlingen salt dome is a mushroom-structured salt body, which is 14 km long and 4–8 km wide extending up to about 4 km depth. Moreover, using equation (5) and knowing the depth and the shape value of the Wathlingen dome, the amplitude coefficient A was found to be $-157.76$ mGal·km$^2$. The observed and the calculated anomalies are shown in Figure 7.

It is evident from the field examples that our method gives good insight concerning the nature of the geology (shape and depth) of salt domes.

## 5. Conclusions

The problem of determining the shape and depth of a buried structure from gravity data can be solved using the present method. A simple and rapid numerical approach is formulated to use the anomaly values at two characteristic points and their corresponding distances on the residual anomaly profile for determining simultaneously the shape and the depth of the buried structure. The repetition of the method using all successful combinations of such pairs of measured points will lead to the best results. The advantages of this statistical method over the least-squares methods are: (1) the method does not require computation of analytical or numerical derivatives with respect to the model parameters, (2) the method is less sensitive to errors in gravity anomaly even when the origin of the anomaly profile is determined incorrectly, and (3) the method does not depended on the anomaly value at the origin in determining the model parameters. In the synthetic examples, the solutions for depth and shape are still in good agreement with the actual model parameters. The maximum error in both model parameters is less than 10%. The method is developed to quantify the shape factor and to determine the depth. In other words, a roughly quantitative shape-related parameter and depth can be derived from gravity data. These two parameters might be used to give a good insight concerning the nature of the geology (shape and depth) of the buried structure.

***Acknowledgements***. The authors would like to thank the editors, particularly, Dr. Igor Kohút and one capable reviewer, for their keen interest and excellent and valuable comments that improved the original manuscript.

## References

Abdelrahman E. M., El-Araby H. M., 1993: Shape and depth solutions from gravity data using correlation factors between successive least-squares residuals. Geophysics, **59**, 1785–1791.

Abdelrahman E. M., El-Araby H. M., 1996: Shape and depth solutions from moving average residual gravity anomalies. Journal of Applied Geophysics, **36**, 23, 89–95.

Abdelrahman E. M., El-Araby H. M., El-Araby T. M., Abo-Ezz E. R., 2001a: Three least-squares minimization approaches to depth, shape, and amplitude coefficient determination from gravity data. Geophysics, **66**, 1105–1109.

Abdelrahman E. M., El-Araby T. M., El-Araby H. M., Abo-Ezz E. R., 2001b: A new method for shape and depth determinations from gravity data. Geophysics, **66**, 1774–1780.

Abdelrahman E. M., Essa K. S., Abo-Ezz E. R., El-Araby T. M., Soliman K. S., 2006: A least-squares variance analysis method for shape and depth estimation from gravity data. Journal of Geophysics and Engineering, **3**, 143–153.

Abdelrahman E. M., Sharafeldin S. M., 1995: A least-squares minimization approach to shape determination from gravity data. Geophysics, **60**, 589–590.

Asfahani J., Tlas M., 2012: Fair function minimization for direct interpretation of residual gravity anomaly profile due to spheres and cylinders. Pure and Applied Geophysics, **169**, 157–165.

Asfahani J., Tlas M., 2015: Estimation of gravity parameters related to simple geometrical structures by developing an approach based on deconvolution and linear optimization techniques. Pure and Applied geophysics, **172**, 2891–2899.

Chakravarthi V., 2011: Automatic gravity optimization of 2.5 D strike listric fault sources with analytically defined fault planes and depth-dependent density. Geophysics, **76**, 2, I21–I31.

Cordell L., Henderson R. G., 1968: Iterative three-dimensional solution of gravity anomaly data using a digital computer. Geophysics, **33**, 596–601.

Essa K., 2007: A simple formula for shape and depth determination from residual gravity anomalies. Acta Geophysica, **55**, 2, 182–190.

Essa K., 2014: New fast least-squares algorithm for estimating the best-fitting parameters due to simple geometric-structures from gravity anomalies. Journal of Advanced Research, **5**, 1, 57–65.

Götze H.-J., Lahmeyer B., 1988: Application of three-dimensional interactive modeling in gravity and magnetic. Geophysics, **53**, 1096-1108.

Dubey C. P., Götze H.-J., Schmidt S., Tiwari V. M., 2014: A 3D model of the Wathlingen salt dome in the Northwest German Basin from joint modeling of gravity, gravity gradient, and curvature. Interpretation, **2**, 4, SJ103–SJ115.

Nandi B. K., Shaw R. K., Agrawal B. N. P., 1997: A short note on identification of the shape of simple causative sources from gravity data. Geophysical Prospecting, **45**, 513–520.

Nettleton L. L., 1976: Gravity and magnetics in oil prospecting. Mc-Graw Hill Book Co. New York.

Nettleton L. L., 1962: Gravity and magnetics for geologists and seismologists. AAPG Bulletin, **46**, 10, 1815–1838.

Shaw R. K., Agarwal S. N. P., 1990: The application of Walsh transform to interpret gravity anomalies due to some simple geometrically shaped causative sources: Feasibility study. Geophysics, **32**, 708–719.

Tanner J. G., 1967: An automated method of gravity interpretation. Geophys. J. Roy. Astor. Soc, **13**, 339–347.

Tlas M., Asfahani J., Karmeh H., 2005: A versatile non-linear inversion to interpret gravity anomaly caused by a simple geometrical structure. Pure and Applied Geophysics, **162**, 12, 2557–2571.